Titre: Title:	Wavelength shift in a whispering gallery microdisk due to bacterial sensing: a theoretical approach
Auteurs: Authors:	Hala Ghali, Pablo Bianucci, & Yves-Alain Peter
Date:	2017
Type:	Article de revue / Article
Référence: Citation:	Ghali, H., Bianucci, P., & Peter, Y.-A. (2017). Wavelength shift in a whispering gallery microdisk due to bacterial sensing: a theoretical approach. Sensing and Bio-Sensing Research, 13, 9-16. https://doi.org/10.1016/j.sbsr.2017.01.004

Document en libre accès dans PolyPublie
Open Access document in PolyPublie

URL de PolyPublie: PolyPublie URL:	https://publications.polymtl.ca/3589/
Version:	Version officielle de l'éditeur / Published version Révisé par les pairs / Refereed
Conditions d'utilisation: Terms of Use:	Creative Commons Attribution-Utilisation non commerciale-Pas d'oeuvre dérivée 4.0 International / Creative Commons Attribution-NonCommercial-NoDerivatives 4.0 International (CC BY-NC-ND)

Document publié chez l'éditeur officiel
Document issued by the official publisher

Titre de la revue: Journal Title:	Sensing and Bio-Sensing Research (vol. 13)
Maison d'édition: Publisher:	Elsevier
URL officiel: Official URL:	https://doi.org/10.1016/j.sbsr.2017.01.004
Mention légale: Legal notice:	

Wavelength shift in a whispering gallery microdisk due to bacterial sensing: A theoretical approach

Hala Ghali [a],[*], Pablo Bianucci [b], Yves-Alain Peter [a]

[a] Department of Engineering Physics, Polytechnique Montréal, H3T 1J4, Canada
[b] Physics Department, Concordia University, Montréal H4B 1R6, Canada

ABSTRACT

Whispering gallery mode microcavities have recently been studied as a means to achieve real-time label-free detection of biological targets such as virus particles, specific DNA sequences, or proteins. Binding of a biomolecule to the surface of a microresonator will increase its path length, leading to a shift in the resonance frequency according to the reactive sensing principle. In this paper, we develop a theoretical expression that will link the reactive shift to the bacteria and microdisk parameters and help quantify the number of bacteria that bind to the surface of a 200μm-diameter silica microdisk.

Crown Copyright © 2017 Published by Elsevier B.V. This is an open access article under the CC BY-NC-ND license (http://creativecommons.org/licenses/by-nc-nd/4.0/).

1. Introduction

Whispering gallery microcavities (WGM) have attracted increased attention in the last decade as tools for label-free biosensing [1–4] and single molecule detection using plasmonic enhancement and optomechanical spring sensing [5–8]. They are structures that can efficiently confine light at the microscale due to total internal reflection of light at the interface between the cavity and its surrounding medium. WGM have a high sensitivity potential due to their high quality factors, as well as being selective when their surface is properly functionalized with the appropriate recognition element, relatively low cost and yield fast response. While the bulk of the research in this field is oriented towards the detection of viruses and small molecules, whispering gallery modes microcavities have a great potential for the detection of bacteria. For instance, *Staphylococcus aureus* (*S. aureus*) is a gram-positive bacterium, which is a common cause of skin and respiratory infections and presents antibiotic-resistant strains such as methicillin-resistant *S. aureus* (MRSA). MRSA is responsible for over 60% of staphylococcal infections in hospitals. It becomes thus crucial to find tools to achieve fast diagnosis and early detection of staphylococcal infections. There exist several techniques that are widely used for this purpose. Bacterial culture is used in most hospitals to identify the presence of *Staphylococcus aureus*. However this kind of tests can take several days to identify the pathogenic bacteria [9]. Real-time PCR is the

most widespread FDA-approved test for MRSA [10,11]. However, this technique is time-consuming (about 2 h), requires prior isolation of bacterial DNA, can be very expensive and is impractical for use on-site or in developing countries. Another study shows the detection of *Staphylococcus aureus* using aptamer-conjugated gold nanoparticles [12]. Although this technique is very sensitive, it can take up to 1.5 h to detect the presence of the bacteria, making it unsuitable for real-time detection. Recently, we have shown the detection of *S. aureus* bacteria in Tris-buffered saline (TBS) (10 mM Tris-HCL, 150 mM NaCl, pH 7.5) by measuring the resonance shifts in silica microdisks which were specifically functionalized to react only to *S. aureus* [13].

2. Materials and methods

2.1. Microdisks fabrication

In this study, optical microdisks are used to detect the presence of bacteria. This particular geometry of optical microcavities was chosen because it can be easily integrated with optics and microfluidics components into a lab on a chip for on-site use, contrary to other microcavity geometries. The microdisks fabricated have a diameter of 200 μm and a 800 nm thickness. The relatively large diameter will decrease the radiation losses inside the disk leading to higher Q factors, whereas the 800 nm thickness was chosen to maximize the confinement of the fundamental energy mode inside the cavity. Optical microdisks are fabricated using standard silicon micromachining
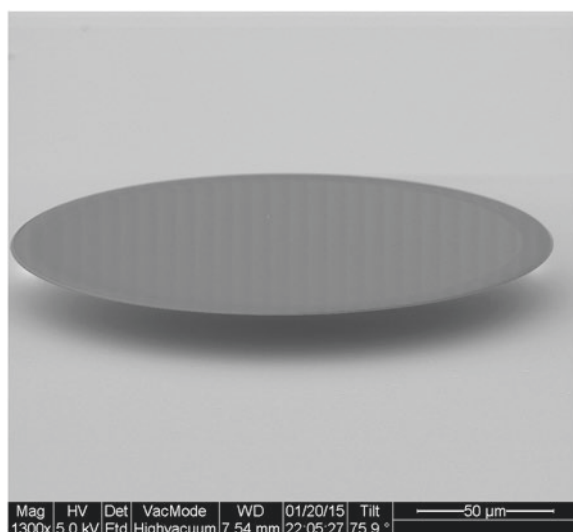
* Corresponding author.

Fig. 1. Scanning electron micrograph of an optical microdisk.

techniques [14]. The substrates used are silicon topped with an 800 nm thermal silicon dioxide layer. The first step performed is UV photolithography to generate photoresist patterns of 200 μm-diameter microdisks with AZ5214 photoresist. Patterns are then transferred to silica using buffered oxide etch (B.O.E.) of silicon dioxide. The last step is isotropic dry etching of silicon with SF_6 gas to obtain microdisks on pedestals. A scanning electron micrograph of a fabricated 200 μm-diameter silica microdisk is shown in Fig. 1.

2.2. Surface functionalization

The functionalization process, needed for the response to be specific to *S. aureus* [15] and shown in Fig. 2 starts by cleaning the microdisks using oxygen plasma to remove organic residues. The

samples are then immersed in an ethanol:water (95:5) solution containing 2.5% triethoxysilane-PEG-NH_2 (Nanocs, MW = 3400) for 2 h, then thoroughly washed with ethanol and dionized water. The PEGylated wafers were then immersed in a 2 μM LysK: 2000 μM EDC (1-Ethyl-3-(3-dimethylaminopropyl)carbodiimide) (1:1000) solution in buffer (10 mM Tris.HCl pH 7.5, 150 mM NaCl, 1% glycerol) at 4 °C overnight, then thoroughly washed with PBS and water.

After the functionalization process, the microdisk surface exposes a layer of LysK, an endolysin from the staphylococcal phage K that binds strongly to staphylococci. It contains three domains: an N-terminal cysteine, a histidine-dependent amidohydrolase/peptidase (CHAP) domain, a midprotein amidase-2 domain, and a C-terminal SH3b cell wall-binding domain [16]. This layer causes approaching bacteria to stick to the surface of the microdisk and then starts lysing their cell membranes. Lysing starts immediately after the addition of *Staphylococcus aureus* to LysK.

2.3. Optical characterization setup

The resonance shifts caused by the binding of bacteria were measured with the experimental setup represented in Fig. 3. Light from a tunable laser source was coupled into a tapered optical fiber next to the 200 μm-diameter silica microdisk, and the transmitted light intensity was measured as the laser wavelength was scanned. The resonances appeared as dips in the transmission spectrum. A typical transmission spectrum of a 200 μm-diameter silica microdisk coupled to a 1.2 μm waist diameter tapered optical fiber is shown in Fig. 4. The quality factor of the microdisks used in this study is around 10^4. This value might seem to be low, but it is common for microdisks, especially when working in an aqueous environment. One method to improve the Q factor is to etch silica using RIE to obtain smoother edges.

Quantitative sensing of the bacterial concentration is important, as a simple presence/absence detection scheme might not be efficient enough in a clinical setting. In this article, we develop a detailed model of the silica microdisks as biosensors in order to quantify the number of detected bacteria based on the measured resonance shifts.

3. Biosensing principle

The biodetection principle has been demonstrated and described in several studies [17,18]. When particles bind to the surface of the microresonator, they interact with its evanescent field, hence increasing the optical path length, leading to a shift towards lower frequencies, i.e. longer wavelengths. This is known as the reactive mechanism for biosensing [19]. The wavelength shift is given by:

$$\frac{\Delta\lambda}{\lambda} = \frac{\Delta R}{R} + \frac{\Delta n}{n}, \tag{1}$$
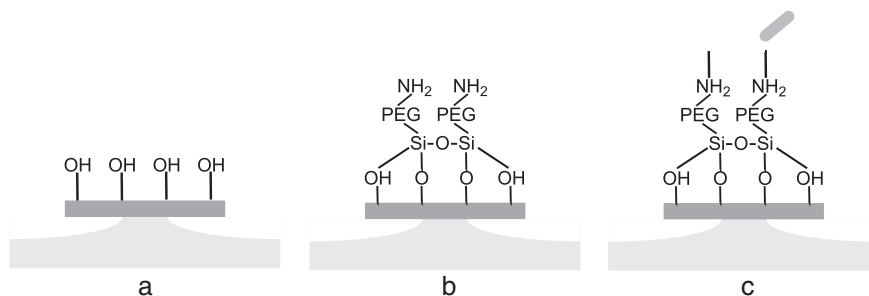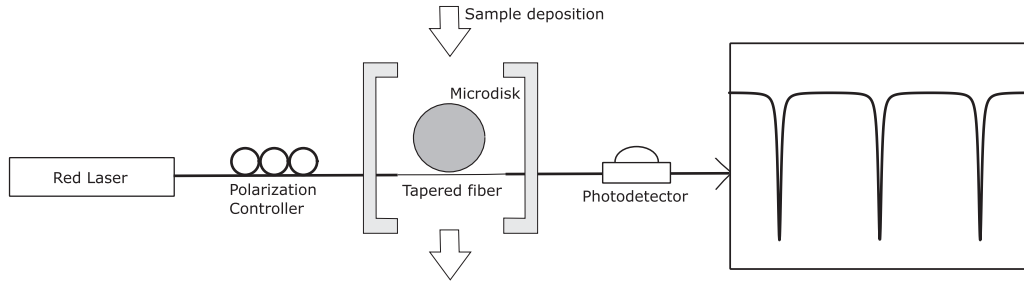

Fig. 2. Functionalization of silica microdisks. (a) The silicon dioxide surface is hydroxylated with oxygen plasma. (b) The disk is immersed in triethoxysilane-PEG-NH_2. (c) The free amines of the PEG-silane are covalently coupled to LysK using carbodiimide coupling.

Fig. 3. Optical characterization setup. The light from a tunable laser at 630nm propagates through a polarization controller and is coupled inside the microdisk using a tapered fiber. The signal conveyed from the photodetector to the oscilloscope yields the transmission spectrum. Resonant modes are observed as a series of dips.

where R is the radius of the microresonator and n its refractive index. For more complex cases where the protein or biomolecules are not uniformly distributed across the resonator surface, the analysis becomes less straightforward. The polarizability of the particles as well as the surface density will have an effect on the resonant wavelength shift [17].

3.1. Theoretical wavelength shift

In order to convert the resonance shifts to more useful information we need a theoretical wavelength shift equation for a microdisk. This formulation allows to determine the surface area covered by the analytes using the experimental wavelength shift, and hence estimate the number or concentration of bacteria that bind to the surface of the disk and contribute to the reactive shift.

The frequency shift caused by the binding of a biomolecule considers the energy of interaction as a first-order perturbation to a single-photon resonant state. When a particle binds at a position $\vec{r}_i$, the resonant shift can be expressed as follows [20]:

$$\left(\frac{\delta\lambda}{\lambda}\right)_i \cong \frac{-\alpha_{ex}\left|\vec{E}_0(\vec{r}_i)^2\right|}{2\int_V \epsilon_s \left|\vec{E}_0(\vec{r})\right|^2 dV}.$$ (2)

The integral in the denominator of Eq. (2) is taken over the microdisk's volume (V). The excess polarizability of the particles binding to the resonator's surface is α_{ex}, while the resonator's dielectric constant is $\epsilon_s = \epsilon_0\epsilon_{rs}$. The addition of equal electric and magnetic contributions is accounted for by adding the factor 2 in front of the integral.

If there is a relatively large number of binding sites with a reasonably uniform distribution, we can approximate the sum in the numerator of Eq. (2) by:

$$\sum_i^N \left|E_0(\vec{r}_i)\right|^2 \cong \sigma_s \int \left|E_0(\vec{r})\right|^2 dA,$$ (3)

with A being the surface area of the resonator and σ_s is the surface area density of the particle covering.
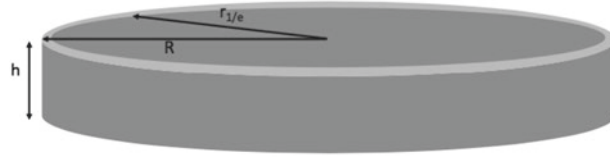
The surface coverage density can be expressed as the number of bound molecules (N) per surface unit as follows:

$$\sigma_s = \frac{N}{\pi\left(R^2 - r_{1/e}^2\right) + 2\pi Rh},$$ (4)

where R is the radius of the microcavity. Eq. (4) considers that bacteria only attach on the top surface of the microdisk. Since the majority of the mode energy is contained on the edge of the microdisk, only bacteria that attach in this region will contribute to the spectral shift. The surface
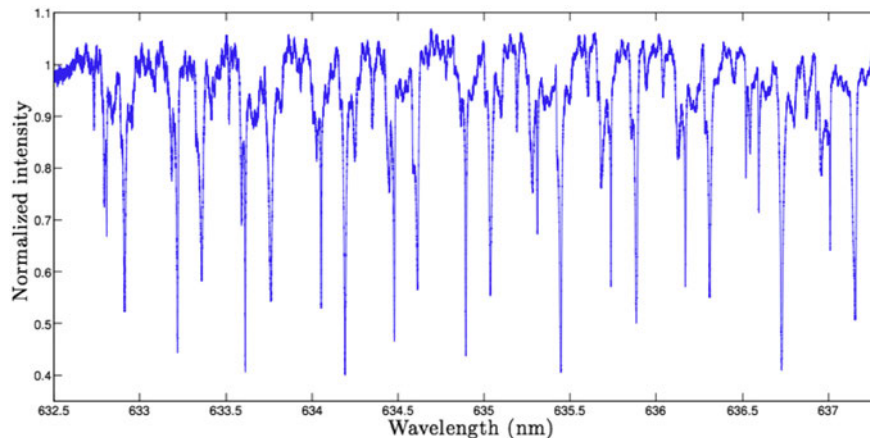
Fig. 4. Transmission spectrum of a 200μm-diameter silica microdisk coupled to a 1.2μm waist diameter tapered optical fiber.

Fig. 5. Schematic representation of the surface area used to calculate the surface coverage density. It is the area where the energy mode of the microdisk is confined, shown in light grey color.

area taken into consideration is then the surface of a ring of outer diameter R where the electric field is maximum, and an inner diameter $r_{1/e}$ where the intensity of the electric field decays to $1/e$ of its maximum, in addition to the surface of the edge, as shown in Fig. 5.

The excess polarizability of the molecules binding to the resonator's surface can be expressed as follows [17]:

$$\alpha_{ex} = 4\pi\epsilon_0 \left(\frac{n_m}{2\pi}\right)\left(\frac{dn_m}{dc}\right)m_{bact},$$ (5)

where n_m is the medium (TBS) refractive index, $\frac{dn_m}{dc} = \lim_{c\to 0}(\frac{n_m - n_0}{c})$, the differential refractive index of molecules in water, where c, is the solvent concentration, and is usually of the order of 0.1 mL/g for polymers in water [21], and m_{bact}, the mass of a single particle.

The only missing piece of information is the spatial distribution of the amplitude of the electric field in the resonator, $\left|\vec{E}(\vec{r})\right|$. We use an analytical approximation to the electric field in a microdisk [22], where the amplitude of the field is separated as follows:

$$E_0 = \Psi(\rho)\Omega(\phi)Z(z) = J_l(k_0 n_m \rho)\exp(im\phi)\exp\left(ik_0\left(\sqrt{n_d^2 - n_m^2}\right)z\right),$$ (6)

where ρ is the microdisk's radius, ϕ represents the angle on the top surface of the disk, k_0 the wavelength number, n_d and n_m the refractive indices of the disk and the medium, respectively, and z the thickness of the resonator, as shown in Fig. 6.

The parameters used to determine the spectral shift due to *S. aureus* binding to a 200 µm-diameter silica microdisk submerged in Tris buffer are defined in Table 1. These values are used for the calculations shown below.

Using Eqs. (2), (3) and (6), the resonant shift for the TE mode of the microdisk can be written as follows:

$$\frac{\delta\lambda}{\lambda} \simeq \frac{\alpha_{ex}\sigma_s}{2\epsilon_0\epsilon_{rs}} \frac{\left[\int_0^R \int_0^{2\pi} |\Psi(\rho)|^2|\Omega(\phi)|^2\left|Z\left(\frac{h}{2}\right)\right|^2\rho d\phi d\rho + \int_0^h\int_0^{2\pi}|\Psi(R)|^2|\Omega(\phi)|^2|Z(z)|^2 R d\phi dz\right]}{\int_0^h\int_0^R\int_0^{2\pi}|\Psi(\rho)|^2|\Omega(\phi)|^2|Z(z)|^2\rho d\phi d\rho dz}.$$ (7)

The integrals in the numerator of Eq. (7) are taken over the top surface of the microdisk and its edge surface respectively. The denominator is the volume integral of the electric field inside the microcavity. The integral of the first-kind Bessel function can be written according to Eq. (8).
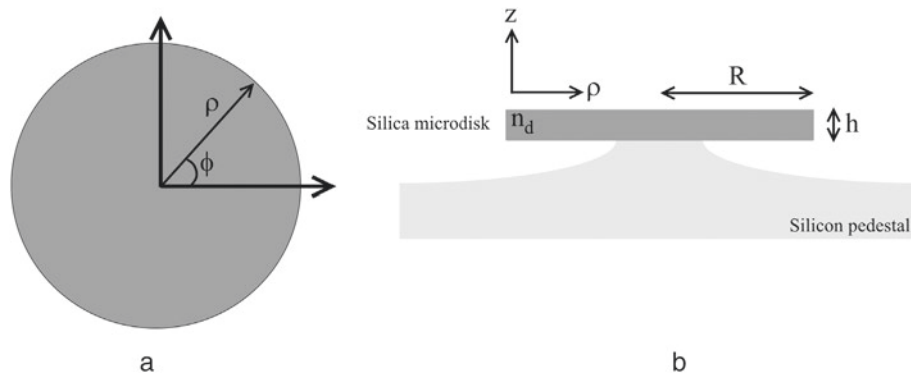
$$\int_0^R [J_l(k_0 n_m \rho)]^2 \rho d\rho = \frac{1}{2}R^2\left[J_{l+1}^2(k_0 n_m R)\right].$$ (8)

The three integrals of Eq. (7) are each solved separately. The first double integral in the numerator is expressed as follows:

$$\int_0^R\int_0^{2\pi}\left|J_l^2(k_0 n_m \rho)\right||\exp(im\phi)|^2\exp^2\left[ik_0\left(\sqrt{n_d^2 - n_m^2}\right)\frac{h}{2}\right]\rho d\phi d\rho = \frac{2\pi}{2}R^2\left[J_{l+1}^2(k_0 n_m R)\right]$$ (9)

The second double integral of the numerator can be expressed as:

$$\int_0^h\int_0^{2\pi}\left|J_l^2(k_0 n_m R)\right||\exp(im\phi)|^2\exp^2\left[ik_0\left(\sqrt{n_d^2 - n_m^2}\right)z\right]R\; d\phi dz = 2\pi R\left[J_l^2(k_0 n_m R)\right]h$$ (10)

Fig. 6. Schematic representation of a fabricated microdisk. a) Top view and b) vertical cut view.

Table 1
Parameters of the wavelength shift equation for a microdisk.

Parameter	Definition	Value
α_{ex}	Excess polarizability	$4\pi\epsilon_0 \times 2.12 \times 10^{-20}$ (m^3)
σ_s	Surface coverage	$\frac{N}{3.78 \times 10^{-9}}$ (m^{-2})
ϵ_0	Vacuum permittivity	8.854×10^{-12} F/m
ϵ_{rs}	Relative permittivity of silica	3.9
k_0	Wavenumber ($\frac{2\pi}{\lambda}$)	9.895×10^6 m^{-1}
n_d	Microdisk refractive index	1.457
n_m	TBS refractive index	1.332
h	Microdisk thickness	800 nm
R	Microdisk radius	100 µm
m_{bact}	Mass of one bacterium	10^{-12} g

with

$$\int_0^h \exp^2\left[ik_0\left(\sqrt{n_d^2 - n_m^2}\right)z\right]dz = h \tag{11}$$

and

$$\int_0^{2\pi} \left|\exp(im\phi)\right|^2 d\phi = 2\pi \tag{12}$$

The denominator of Eq. (7) is calculated as follows:

$$\int_0^h \int_0^R \int_0^{2\pi} \left|J_l^2(k_0 n_m \rho)\right| \left|\exp(im\phi)\right|^2 \exp^2\left[ik_0\left(\sqrt{n_d^2 - n_m^2}\right)z\right]\rho\,d\phi\,d\rho\,dz = \frac{1}{2}R^2\left[J_{l+1}^2(k_0 n_m R)\right]h\int_0^{2\pi}\left|\exp(im\phi)\right|^2 d\phi \tag{13}$$

The integral part (I) of the spectral shift equation (Eq. (7)) can be grouped and simplified as follows:

$$I = \frac{R\left[J_{l+1}^2(k_0 n_m R)\right] + 2h\left[J_l^2(k_0 n_m R)\right]}{Rh\left[J_{l+1}^2(k_0 n_m R)\right]} = \frac{1}{h} + \frac{2\left[J_l^2(k_0 n_m R)\right]}{R\left[J_{l+1}^2(k_0 n_m R)\right]} \tag{14}$$

With an explicit expression for the integral in Eq. (7) in hand, we can then use Eq. (2) to find out an expression for the spectral shift. This expression is an approximation rather than an exact solution because there is no exact solution to the modes of a microdisk. Furthermore, microdisks are considered as 2D structures, and only the bacteria that bind to the edge of the microresonator are taken into account to calculate the wavelength shift. The resonance shift for a WGM microdisk can then be estimated by the following equation:

$$\frac{\delta\lambda}{\lambda} \simeq \frac{\alpha_{ex}\sigma_s}{2\epsilon_0\epsilon_{rs}}\left\{\frac{1}{h} + \frac{2\left[J_l^2(k_0 n_m R)\right]}{R\left[J_{l+1}^2(k_0 n_m R)\right]}\right\} \tag{15}$$

As can be seen in Eq. (15), the wavelength shift depends on the radius of the microdisk and is not affected by its Q-factor. This relationship can hence be applied to all optical microdisks of different sizes and Q-factors.

Simulations using a Finite-Difference-Time-Domain (FDTD) program, MEEP, were performed to observe the effect of a binding event that occurs on the surface of a microdisk on the wavelength shift. The 3D simulations considered the 100 µm-radius microdisk as a cylindrically symmetric geometry and the 2 µm-diameter bacterium as a torus shape. A cross-section of the microcavity and the bacterium is shown in Fig. 7. The parameters used are presented in Table 1. The position of the bacterium was varied between 90 and 100 µm from the center of the microdisk. As can be seen in Fig. 8, with the change in radial position the wavelength shift increases, with a maximum shift occurring at 99.2 µm from the center of the microdisk. As explained above, most of the electrical field that interacts with a binding particle is confined on
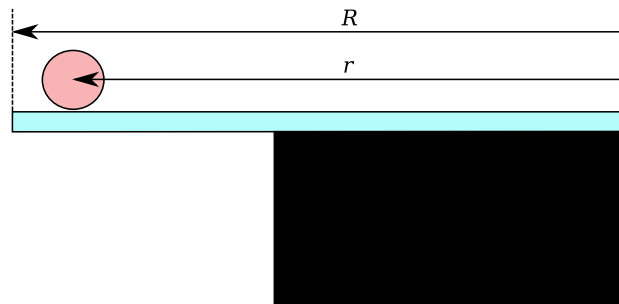
Fig. 7. Cross-section of the microdisk and the bacterium situation used for the FDTD simulations. On the figure, black is silicon, light blue is the microdisk and pink is the bacterium. R is the disk radius and r the bacterium radial position.
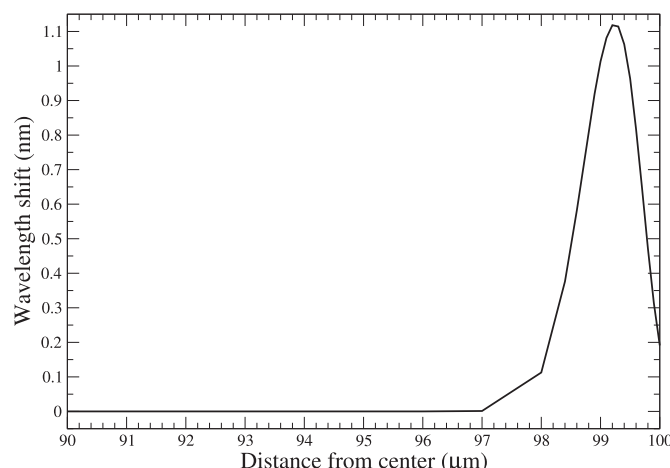
Fig. 8. Spectrum showing the wavelength shift variation for different radial positions of the bacterium. A maximum wavelength shift is observed for a bacterium that binds at 99.2μm from the center of the microdisk.

the edge of the microdisk, more specifically at the surface area chosen to find the surface coverage density in Eq. (4). The results obtained from these simulations further assert this choice of surface area and thus confirm that a bacterium binding to the surface of the microdisk where the electric field is at its maximum will indeed increase the wavelength shift, as predicted by Eq. (15). Considering that bacteria binding to the surface of the microdisk form a ring on it, the maximum number of bacteria would approximately be 314 bacteria contributing to the maximum shift of 1.1 nm shown in Fig. 8. The shift per bacterium can thus be extrapolated and estimated around 3.5 pm at 605 nm wavelength. The wavelength shift corresponding to the binding of 40 bacteria would be around 2.3×10^{-4}, the same order of magnitude as the shift found theoretically from Eq. (15), and shown in Fig. 11.

3.2. Experimental results

Bacteria were added to the surface of a functionalized silica microdisk using a micropipette. As soon as the bacteria stick to the surface of the microdisk, LysK phage starts immediately lysing the *Staphylococcus aureus*. It takes about 30 min for most of the bacteria to be lysed. A graph showing the variation of the wavelength shift in time after the binding of *S. aureus* to the surface of an optical microdisk is shown in Fig. 9, confirming the behaviour predicted by Eq. (15) and shown in Fig. 8.
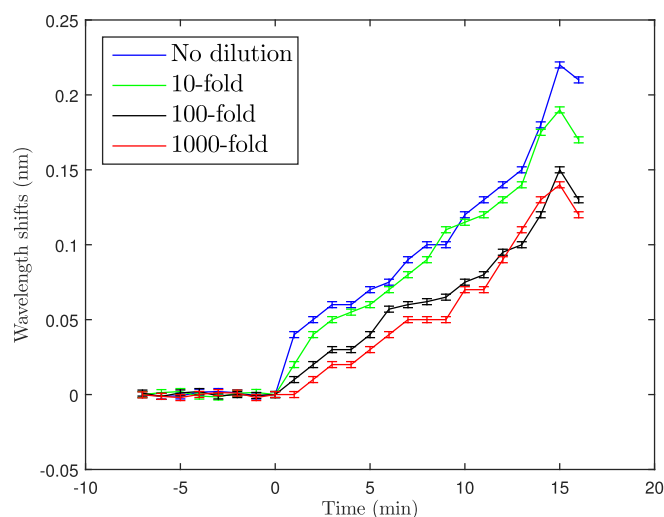
Four different concentrations of bacteria were used experimentally, leading to four different wavelength shifts [13]. Fig. 10 shows the maximum wavelength shifts obtained experimentally for the four different concentrations. From these wavelength shifts, the corresponding number of bacteria that bind to the surface of the resonator in each case was calculated using Eq. (15). The results are summarized in Table 2 and plotted on Fig. 11. Contrary to what would be expected, the number of bound bacteria found experimentally is not proportional to the initial solution concentration. Since the microdisks used were functionalized identically, the same maximum value of the wavelength shift is expected since the bacterial cells would saturate all of the available sites. However, for dilute solutions, the bacteria will be depleted before all of the binding sites become saturated. Furthermore, not all the active protein sites are located on the sensitive part of the disk where the energy mode is at its highest, which leads to a variability in the number of bound bacteria that contribute to the wavelength shift.

The minimum shift that could be observed was of 0.14 nm, corresponding to 30 bacteria binding to the surface of the microresonator and contributing to the spectral shift. The bacterial concentration used in this case was 5.10^6 CFU/mL.
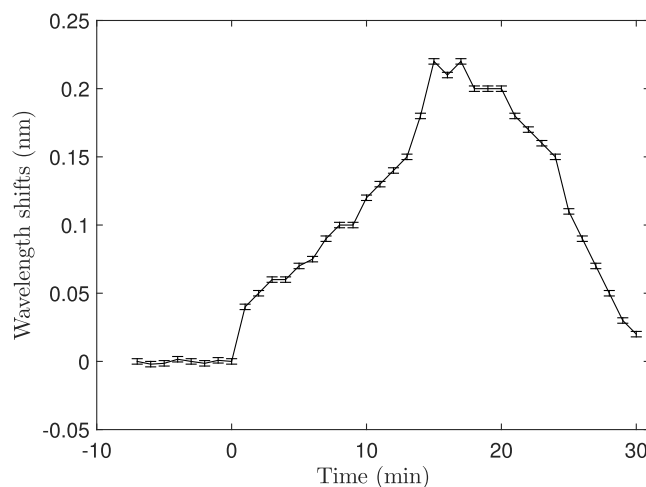
Fig. 9. Wavelength shift in time after *S. aureus* binding to the resonator. A buffer solution is added to the surface of the microdisk using a micropipette. At time T = 0, the same buffer containing *S. aureus* bacteria is added. Error bars are due to uncertainties in the values resulting from laser drift and error in calculating the shift from the transmission spectra (±2 pm).

Fig. 10. Wavelength shifts after *S. aureus* binding for four different concentrations. A buffer solution is added to the surface of the microdisks using a micropipette. At time T = 0, the same buffer containing four different concentrations of *S. aureus* bacteria is added to the microdisks. Error bars are due to uncertainties in the values resulting from laser drift and error in calculating the shift from the transmission spectra (± 2 pm).
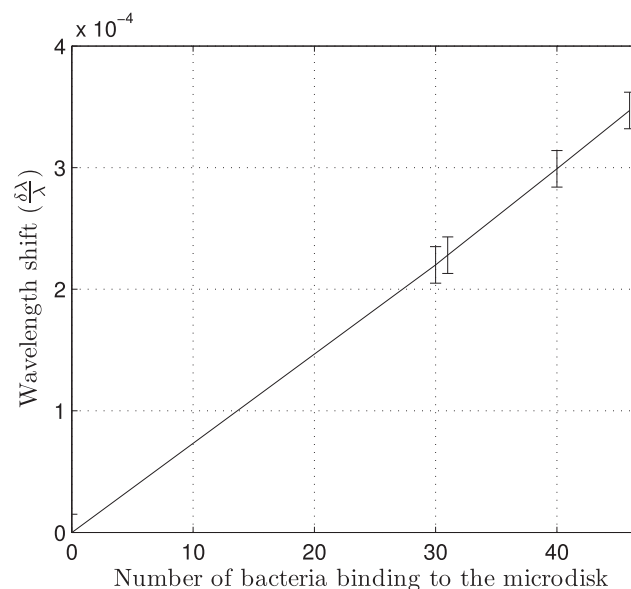
Fig. 11 is a graphical representation of the theoretical wavelength shift relationship of Eq. (15). It shows the variation of the theoretical wavelength shift versus the number of bacteria that bind to the surface of a 200 μm-diameter silica microdisk with a $Q = 10^4$, found from Eqs. (4) and (15). As can be observed in Fig. 11, the spectral shift varies linearly with the number of bacteria that attach to the surface of a microdisk. Accordingly, an extrapolation shows that the binding of a single bacterium is expected to cause a shift of 5 pm, the same order of magnitude as the shift per bacterium predicted by the FDTD simulations discussed in Section 3.1. Since the shift caused by the attachment of a single bacterium is relatively small, it becomes crucial to have a stabilized optical characterization setup to avoid the effects of laser instabilities or temperature changes on the spectral shift. The thermal spectral shift for a cavity resonance wavelength of 635 nm is equal to 3.81 pm/°C. A method to control the temperature could be to use a Peltier heat pump device and thermistor that could control the temperature to 0.01 °C [23]. Another method could be the use of thermal-stabilized reference interferometer with a high-Q optical microcavity [24]. This could enhance the signal to noise ratio and allow to have a highly sensitive biosensor. The use of appropriate microfluidic channels could also ensure that the bacterium binds to the edge of the microdisk that contains most of the mode energy so it could be accurately detected.

4. Conclusion

In this work, we have developed an equation to estimate the number of bacteria that bind to a 200 μm-diameter silica microdisk from the wavelength shift observed experimentally. This expression has allowed us to find a limit of detection for *Staphylococcus aureus* of 5 pg/mL for a microdisk with $Q = 10^4$, corresponding to 30 cells. The theoretical expression of the wavelength shift developed in this work can be applied more generally to find the spectral shift that results from the binding of any biological particle on the surface of an optical microdisk. It is important however to use the appropriate parameters corresponding to these particles while calculating their excess polarizability in order to obtain an accurate result. It is believed that using microdisks with higher quality factors combined with an adequate and stabilized optical characterization setup so that environmental changes don't affect the biosensing process, would allow real-time single bacterium detection using optical microdisks.

Conflict of interest

The authors don't have any conflict of interest.

Fig. 11. A graphical representation of the theoretical wavelength shift relationship of Eq. (15) in terms of number of bacteria contributing to the shift. The graph shows the variation of the wavelength shift versus the number of bacteria that bind to the surface of a 200 μm-diameter silica microdisk with a $Q = 10^4$, found from Eqs. (4) and (15).

Table 2
Number of bacteria binding to the resonator for four different concentrations.

Bacterial solution concentration (CFU/mL)	Wavelength shift ($\delta\lambda$ in nm)	Bacteria bound to the surface
5×10^9	0.22	46
5×10^8	0.19	40
5×10^7	0.15	31
5×10^6	0.14	30

Acknowledgments

References

[1] K.J. Vahala, Optical microcavities, Nature 424 (6950) (2003) 839–846.

[2] N. Massad-Ivanir, G. Shtenberg, A. Tzur, M.A. Krepker, E. Segal, Engineering nanostructured porous sio2 surfaces for bacteria detection via direct cell capture, Anal. Chem. 83 (9) (2011) 3282–3289.

[3] X. Lopez-Yglesias, J.M. Gamba, R.C. Flagan, The physics of extreme sensitivity in whispering gallery mode optical biosensors, J. Appl. Phys. 111 (8). (2012) 084701–084701.

[4] M.R. Foreman, J.D. Swaim, F. Vollmer, Whispering gallery mode sensors, Adv. Opt. Photon. 7 (2) (2015) 168–240.

[5] S. Shopova, R. Rajmangal, S. Holler, S. Arnold, Plasmonic enhancement of a whispering-gallery-mode biosensor for single nanoparticle detection, Appl. Phys. Lett. 98 (24) (2011) 243104.

[6] M.D. Baaske, M.R. Foreman, F. Vollmer, Single-molecule nucleic acid interactions monitored on a label-free microcavity biosensor platform, Nat. Nanotechnol. 9 (11) (2014) 933–939.

[7] W. Yu, W.C. Jiang, Q. Lin, T. Lu, Coherent optomechanical oscillation of a silica microsphere in an aqueous environment, Opt. Express 22 (18) (2014) 21421–21426.

[8] W. Yu, W.C. Jiang, Q. Lin, T. Lu, Cavity optomechanical spring sensing of single molecules, Nat. Commun. 7 (2016)

[9] D. Ivnitski, I. Abdel-Hamid, P. Atanasov, E. Wilkins, Biosensors for detection of pathogenic bacteria, Biosens. Bioelectron. 14 (7) (1999) 599–624.

[10] J.-C. Cheng, C.-L. Huang, C.-C. Lin, C.-C. Chen, Y.-C. Chang, S.-S. Chang, C.-P. Tseng, Rapid detection and identification of clinically important bacteria by high-resolution melting analysis after broad-range ribosomal RNA real-time PCR, Clin. Chem. 52 (11) (2006) 1997–2004.

[11] S. Van Hal, D. Stark, B. Lockwood, D. Marriott, J. Harkness, Methicillin-resistant staphylococcus aureus (MRSA) detection: comparison of two molecular methods (IDI-MRSA PCR assay and genotype MRSA direct PCR assay) with three selective MRSA agars (MRSA ID, MRSASelect, and CHROMagar MRSA) for use with infection-control swabs, J. Clin. Microbiol. 45 (8) (2007) 2486–2490.

[12] Y.-C. Chang, C.-Y. Yang, R.-L. Sun, Y.-F. Cheng, W.-C. Kao, P.-C. Yang, Rapid single cell detection of Staphylococcus aureus by aptamer-conjugated gold nanoparticles, Sci. Rep. 3 (2013)

[13] H. Ghali, H. Chibli, J.L. Nadeau, P. Bianucci, Y.-A. Peter, Real-time detection of Staphylococcus aureus using whispering gallery mode optical microdisks, Biosensors 6 (2) (2016) 20.

[14] S. Bergeron, F. Vanier, Y.-A. Peter, Silica Microdisk Coupled Resonator Optical Waveguide, Optical MEMS and Nanophotonics, 2009 IEEE/LEOS International Conference on, IEEE, 2009, pp. 73–74.

[15] H. Chibli, H. Ghali, S. Park, Y.-A. Peter, J.L. Nadeau, Immobilized phage proteins for specific detection of staphylococci, Analyst 139 (1) (2014) 179–186.

[16] S.C. Becker, J. Foster-Frey, D.M. Donovan, The phage k lytic enzyme lysk and lysostaphin act synergistically to kill MRSA, FEMS Microbiol. Lett. 287 (2) (2008) 185–191.

[17] F. Vollmer, D. Braun, A. Libchaber, M. Khoshsima, I. Teraoka, S. Arnold, Protein detection by optical shift of a resonant microcavity, Appl. Phys. Lett. 80 (21) (2002) 4057–4059.

[18] S. Arnold, S. Shopova, S. Holler, Whispering gallery mode bio-sensor for label-free detection of single molecules, thermo-optic vs. reactive mechanism, Opt. Express 18 (1) (2010) 281–287.

[19] F. Vollmer, S. Arnold, D. Keng, Single virus detection from the reactive shift of a whispering-gallery mode, Proc. Natl. Acad. Sci. 105 (52) (2008) 20701–20704.

[20] S. Arnold, M. Khoshsima, I. Teraoka, S. Holler, F. Vollmer, Shift of whispering–gallery modes in microspheres by protein adsorption, Opt. lett. 28 (4) (2003) 272–274.

[21] T. Tumolo, L. Angnes, M.S. Baptista, Determination of the refractive index increment (dn/dc) of molecule and macromolecule solutions by surface plasmon resonance, Anal. Biochem. 333 (2) (2004) 273–279.

[22] M. Borselli, T. Johnson, O. Painter, Beyond the rayleigh scattering limit in high-q silicon microdisks: theory and experiment, Opt. Express 13 (5) (2005) 1515–1530.

[23] C.A. Barrios, K.B. Gylfason, B. Sánchez, A. Griol, H. Sohlström, M. Holgado, R. Casquel, Slot-waveguide biochemical sensor, Opt. lett. 32 (21) (2007) 3080–3082.

[24] T. Lu, H. Lee, T. Chen, S. Herchak, J.-H. Kim, S.E. Fraser, R.C. Flagan, K. Vahala, High sensitivity nanoparticle detection using optical microcavities, Proc. Natl. Acad. Sci. 108 (15) (2011) 5976–5979.